https://doi.org/10.1016/j.ceramint.2019.03.254

Transformation of Hardening to Softening Behaviors Induced by Sb Substitution in CuO-Doped KNN-Based Piezoceramics

You Liao[1], Dongmei Wang[1], Hua Wang[1], Tao Wang[1], Qiaoji Zheng[1], Jiahui Yang[2], K. W. Kwok[3] and Dunmin Lin[1,*]

[1]College of Chemistry and Materials Science, Sichuan Normal University, Chengdu 610066, China

[2]Btuker (Beijing) Scientific Technology Co., Ltd, Shanghai 200233, China

[3]Department of Applied Physics and Materials Research Centre, The Hong Kong Polytechnic University, Kowloon, Hong Kong, China

[*] Corresponding author: Email: ddmd222@sicnu.edu.cn (Dunmin Lin); Fax: +86 28 84760802 Tel: +86 28 84760802

Abstract

Pb-free piezoceramics of $K_{0.5}Na_{0.5}Nb_{1-x}Sb_xO_3$ + 1 mol% CuO are synthesized via a solid-state reaction. Furthermore, the transformation of hardening to softening behaviors induced by Sb substitution is exhibited and the corresponding microscopic mechanism is proposed. The CuO-doped $K_{0.5}Na_{0.5}NbO_3$ ceramic without adding Sb exhibits extremely hardening characteristics (i.e., ultrahigh Q_m of ~2426, low *tan*δ of 0.32%, and pinched ferroelectric hysteresis loop) due to the formation of defect combinations ($(Cu_{Nb}''' - V_O^{\bullet\bullet})'$ and $(V_O^{\bullet\bullet} - Cu_{Nb}''' - V_O^{\bullet\bullet})^{\bullet}$). Whereas, the addition of Sb dramatically reduces the levels of defect combinations, leading to obviously softening properties (d_{33} > 210 pC N^{-1}, k_p > 40%, low Q_m, and normal single *P*-*E* hysteresis loop). Our results indicate that the decrease of defect combinations with Sb addition should be responsible for the hardening-softening transformation of piezoelectricity and ferroelectricity in CuO-doped $K_{0.5}Na_{0.5}Nb_{1-x}Sb_xO_3$ piezoceramics.

Keywords: KNN ceramic; hardening property; softening property; defect structure

1. Introduction

Defect engineering is regarded as an important strategy for material modification.[1] For perovskite piezoelectric materials, adding dopants to induce the formation of defect structures is frequently used to regulate their electric properties.[2-4] Donor doping (high-valence substitution) can induce cation vacancies to enhance the activity of ferroelectric domains, improving the piezoelectric constant d_{33}. For example, softening Pb(Ti, Zr)O_3-based piezoceramics have been widely studied by introducing high valent ions of Ta^{5+}, Nb^{5+} or La^{3+} entering into $(Zr, Ti)^{4+}$ or Pb^{2+} sites, forming $Ta_{Ti}^{\bullet}$, $Nb_{Ti}^{\bullet}$ or $La_{Pb}^{\bullet}$ defects.[5-8] Contrarily, acceptor doping (low-valence substitution) can facilitate the generation of oxygen vacancies and even promote the recombination of defect dipoles, which can significantly improve the mechanical quality factor Q_m of the ceramics as a result of the pining effect of defect dipoles.[9] Such hardening Pb(Ti, Zr)O_3-based piezoceramics have been developed by forming defect dipoles (e.g., $(Fe'_{Zr/Ti} - V_O^{\bullet\bullet})^{\bullet}$, $(Cu''_{Zr/Ti} - V_O^{\bullet\bullet})^{\times}$, and $(Mn''_{Zr/Ti} - V_O^{\bullet\bullet})^{\times}$) using some low valent ions (e.g., Fe^{3+}, Cu^{2+}, and Mn^{2+} ions) to replace $(Zr, Ti)^{4+}$ ions.[10-12]

In recent years, Pb-free piezoceramics have raised considerable spotlight due to the concerns of ecological environment and human health.[13, 14] Among numerous Pb-free piezoelectric systems, $K_{0.5}Na_{0.5}NbO_3$ (KNN) Pb-free piezoceramics doped with acceptor ions, such as Cu, Mn, and Fe ions, have been extensively studied for obtaining hardening properties which are demanded for high-power applications.[15, 16] In particular, among commonly used acceptor dopants, Cu-containing compounds

can induce the most hardening characteristics (super-high Q_m, almost completely constricted *P-E* hysteresis loop, and large internal bias field E_i) in KNN ceramics. For perovskite KNN ceramics, Cu^{2+} can induce the generation of two kinds of defect combinations, namely, binary defect combination $(Cu_{Nb}''' - V_O^{\bullet\bullet})'$ and ternary defect combination $(V_O^{\bullet\bullet} - Cu_{Nb}''' - V_O^{\bullet\bullet})^{\bullet}$. In these two defect combinations, $(Cu_{Nb}''' - V_O^{\bullet\bullet})'$ is considered as the main origin of the hardening performance of the material due to its larger electric dipole moment which supplies a strong releasing force on ferroelectric domains.[17-19] Therefore, the introduction of a large number of defect dipoles leads to a significant enhancement in hardening performance with super-high Q_m (>2000) and completely constricted *P-E* hysteresis loop. However, as shown in **Table 1**, such hardening effect can't be detected in the modified KNN ceramics reported in various literatures[19-26], indicating that the introduction of CuO into Sb, Ta and/or ABO_3-type perovskite-modified KNN materials doesn't lead to obvious hardening piezoelectric and ferroelectric behaviors. This is very interesting and confusing, and its microscopic mechanism hasn't been clearly understood. In this work, we synthesized CuO-doped $K_{0.5}Na_{0.5}Nb_{1-x}Sb_xO_3$ piezoceramics (KNNSC-*x*) and studied their evolution of piezoelectricity and ferroelectricity with the addition of Sb. This study reveals that the introduction of Sb significantly decreases the levels of two sorts of defect combinations and thus results in the transformation of hardening to softening behaviors in KNNSC-*x* piezoceramics. Clearly, this research provides deep insights for the correlation between defect structures and ferroelectric/piezoelectric behaviors in KNN-based piezoceramics.

Table 1. Piezoelectric constant d_{33} and mechanical quality factor Q_m of KNN-based ceramics doped with Sb/Ta/Cu.

Composition	d_{33} (pC N^{-1})	Q_m	Reference
$K_{0.5}Na_{0.5}NbO_3$	125	71	[19]
$K_{0.5}Na_{0.5}NbO_3$ + 1 mol% CuO	83	2235	[19]
$(K_{0.5}Na_{0.5})(Nb_{0.92}Sb_{0.03}Ta_{0.05})O_3$ + 2-3 mol% CuO	130	1134	[20]
$(Na_{0.535}K_{0.485})_{0.93}Li_{0.07}(Nb_{0.942}Ta_{0.058})O_3$ + l mol% CuO	185	323	[21]
$0.95(K_{0.5}Na_{0.5}NbO_3)$–$0.05Li(Nb_{0.5}Sb_{0.5})O_3$ + 0.8 mol% CuO	207	320	[22]
$K_{0.5}Na_{0.5}Nb_{0.93}Sb_{0.07}O_3$ + 1.5 mol% CuO	150	206	[23]
$0.94(K_{0.48}Na_{0.535})NbO_3$–$0.06LiNbO_3$ + 1 mol% CuO	157.5	173.5	[24]
$K_{0.5}Na_{0.5}Nb_{0.91}Sb_{0.09}O_3$ + 1 mol% CuO	230	102	[25]
$0.95Na_{0.5}K_{0.5}NbO_3$–$0.05LiSbO_3$ + 0.45 mol% CuO	175	41.5	[26]

2. Experimental Section

2.1 Sample preparation

$K_{0.5}Na_{0.5}Nb_{1-x}Sb_xO_3$ + 1 mol% CuO Pb-free piezoceramics with x = 0-0.16 were produced via a typical ceramic technique. Chemical reagents K_2CO_3 (99.5%, Sinopharm), Na_2CO_3 (99.8%, Sinopharm), Nb_2O_5 (99.99%, Sinopharm), Sb_2O_3 (99%, Sinopharm), and CuO (99%, Sinopharm) were adopted as initial materials. $K_{0.5}Na_{0.5}Nb_{1-x}Sb_xO_3$ (KNNS) powders were prepared by calcining at 880 ^oC for 6 h after 8 h of ball-milling in ethanol. Afterwards, KNNS powders were mixed with 1

mol% CuO in ethanol through ball-milling for another 8 h. Then the resulting powder was blended with a PVA binder (10 wt%) after drying in an oven and shaped into disk with a diameter of ~11.6 mm and a thickness of ~1.1 mm. After the exclusion of PVA at 650 ^{o}C, green disks were sintered at 1080 °C for 4 h (air atmosphere). Silver electrodes were covered on the ceramic surface at 650 °C. Some obtained samples were poled at 100 °C for 30 min (silicon oil bath) in a DC field (E = 4 kV mm^{-1}).

2.2 Structure and performance characterizations

The phase structures were examined by an X-ray diffractometer (SmartLab, Rigaku, Japan). And the XRD patterns were analyzed with Rietveld refinement method using GSAS-EXPGUI software package.[27, 28] The surface microstructure was observed using a SEM (FEI-Quanta 250, FEI, Netherlands), while the fracture sections of the ceramics were thermally etched at 1060 °C for 1 h after polishing and then observed using a SEM (SU3500, Hitachi, Japan). The temperature-dependent dielectric loss *tan*δ and relative dielectric permittivity ε_r were obtained using an LCR meter (Agilent E4980A, Agilent Technologies Inc, Malaysia). *P-E* and *I-E* hysteresis loops were measured by a ferroelectric test system (Premier II, Radiant technologies Inc, USA). X-band (9.4 GHz) EPR spectra were performed at 90 K with an EPR spectrometer (E580, Bruker, Germany) and fitted using Elexsys Xepr software package.[19] XPS spectra were performed by an X-ray photoelectron spectrometer (ESCALAB 250XI, Thermo Scientific, China) and the binding energy was calibrated with C 1*s* (284.8 eV).[29] The d_{33} was obtained using a piezo-d_{33} meter (ZJ-6A, Chinese Academic

Society, China). The Q_m and k_p were calculated by the resonance and antiresonance method.[30]

3. Results and discussion

3.1 Phase structure and microtopography

Figure 1a exhibits the XRD spectra of KNNSC-*x* ceramics. As $x \leq 0.08$, the ceramics present a perovskite structure without impurity phases, implying that both Sb^{5+} and Cu^{2+} ions have successfully dissolved into KNN lattice. However, a small amount of impurity phase ($K_2NaSb_3O_9$) is detected in KNNSC-0.16 ceramic probably due to the solubility limit of Sb in KNN. Similar formation of impurity phases induced by excessive Sb (≥ 10 mol%) has been reported in KNN-based ceramics.[31, 32] It is worth noting that the two diffraction peaks of (202) and (020) gradually shift closely and merge into a single one as *x* increases to 0.16, implying that KNNSC-*x* ceramics exhibit phase evolutions after the displacement of Sb^{5+} for Nb^{5+}. Similar phase transformation phenomena have been observed in Ta/Sb-doped KNN piezoceramics.[32-34] For purpose of understanding the phase transformation in KNNSC-*x* ceramics, the XRD patterns (2θ = 44-48°) are fitted by Lorentz function, as displayed in **Figure 1**b. The ceramics doped with a small amount of Sb ($x \leq 0.04$) exhibit an orthorhombic symmetry (O phase) with a sharp split between the two peaks of (202) and (020). Nevertheless, the diffraction peak of rhombohedral symmetry (R phase) is observed in KNNSC-0.08 ceramics, indicating the coexistence of O and R phases in this component. Furthermore, R phase gradually increases with further

increasing x (e.g., x = 0.16). That is, the crystal phases of KNNSC-x ceramics transform from O phase to R phase as the level of Sb doping increases.

Table 2. Crystal structure parameters, fitting parameters and relative densities for KNNSC-x ceramics.

Sample	*SG*	α (= β= γ)	a (Å)	b (Å)	c (Å)	V (Å^3)	R_{wp}	R_p	χ^2	R_D (%)
x = 0	*Amm2*	90^o	3.947598	5.645963	5.677159	126.533	0.068	0.0524	1.684	96.59±0.05
x = 0.01	*Amm2*	90^o	3.951944	5.645453	5.673413	126.577	0.0541	0.0396	1.906	97.22±0.05
x = 0.02	*Amm2*	90^o	3.949258	5.637379	5.663757	126.095	0.0511	0.0377	1.840	97.33±0.05
x = 0.04	*Amm2*	90^o	3.954410	5.634856	5.656759	126.047	0.0448	0.0329	1.315	97.91±0.05
x = 0.08	*Amm2*	90^o	3.956023	5.622666	5.639597	125.444	0.0372	0.0266	0.919	97.48±0.05
	R3m: R	89.944^o	3.978685	3.978685	3.978685	62.982				
x = 0.16	*Amm2*	90^o	3.972691	5.598200	5.590162	124.325	0.0464	0.0348	1.297	97.25±0.05
	R3m: R	90.061	3.968850	3.968850	3.968850	62.516				

The Rietveld refinement of XRD patterns is performed with virginal models of O phase ($K_{0.5}Na_{0.5}NbO_3$, *Amm2*), R phase ($KNbO_3$, *R3m: R*), and impurity phase ($K_2NaSb_3O_9$, *Pn-3Z*).[35-38] The patterns of Rietveld refinement are displayed in **Figure 2**a-f, while the crystal structure parameters and fitted parameters are listed in **Table 2**. The fitting parameters R_{wp}, R_p, and χ^2 are less than 6.8%, 5.24%, and 1.906, respectively, indicating that the refinement results match the observed patterns fairly well. The cell volumes gradually decrease with x increasing, demonstrating that the

replacement of Sb^{5+} ions for Nb^{5+} ions leads to the lattice shrinkage owing to a smaller ionic radius of Sb^{5+} (0.60 Å) than Nb^{5+} (0.64 Å).[38, 39] In addition, these refinement parameters further confirm the O-R phase evolution with the addition of Sb.

The temperature dependences of ε_r and *tan*δ for KNNSC-*x* piezoceramics are shown in **Figure 2**g-h and **Figure S1** (Supplemental Information). All ceramics exhibit three dielectric peaks in the temperature range of -150-500 ^oC. The dielectric peak at low temperature (see **Figure S1**) belongs to ferroelectric rhombohedral-ferroelectric orthorhombic phase transition ($T_{R\text{-}O}$).[32] Meanwhile, a sharp peak and a stepped peak are observed at T = 50-500 ^oC, respectively: the sharp peak belongs to tetragonal-cubic phase transition (T_C), while the stepped one belongs to orthorhombic-tetragonal phase transition ($T_{O\text{-}T}$).[23, 40] As shown in the phase diagram (**Figure 2**i), it's evident that, with the increasing content of Sb, both T_C and $T_{O\text{-}T}$ drop step by step, while $T_{R\text{-}O}$ slowly goes up. Concretely, the $T_{R\text{-}O}$ and $T_{O\text{-}T}$ of KNNSC-0.08/KNNSC-0.16 ceramics are 15 ^oC/26 ^oC and 135 ^oC/119 ^oC, respectively, verifying that R and O phases coexist at room temperature in KNNSC-*x* ceramics with $x \geq 0.08$.

Figure 3 shows the microstructure of thermally etched cross section after polishing and the surface (inserts) of KNNSC-*x* ceramics. Similar to other reports of Sb-doped KNN-based ceramics[32, 41, 42], the doping content of Sb significantly affects the grain size of KNNSC-*x* ceramics. For the KNNSC-0 ceramics, the grains are highly uniform and relatively small. However, when little amounts of Sb ($x < 0.08$) are added,

larger grains appear. Nevertheless, smaller and more uniform grains are noticed in KNNSC-*x* ceramics modified by high content of Sb ($x \geq 0.08$), illustrating that excess Sb can inhibit the grain growth which can be ascribed to the emerge of impurity ($K_2NaSb_3O_9$). As provided in **Table 2**, after adding Sb, the relative density of ceramics is raised above 97%, suggesting that the doping of Sb can improve the densification of ceramics.

3.2 Microscopic defect structures

The X-band EPR spectra of KNNSC-*x* ceramics are exhibited in **Figure 4**a. Similar to CuO-doped Pb-based ceramics[43, 44], the replacement of Cu^{2+} for B-site ions leads to the increase of oxygen vacancies $V_O^{\bullet\bullet}$ for charge balance and these Cu^{2+} ions are further associated with $V_O^{\bullet\bullet}$ to constitute defect combinations.[45] Dissimilarly, KNN-based ceramics doped with CuO usually obtain two sorts of defect combinations, i.e., the dimeric $(Cu_{Nb}''' - V_O^{\bullet\bullet})'$ and trimeric $(V_O^{\bullet\bullet} - Cu_{Nb}''' - V_O^{\bullet\bullet})^{\bullet}$.[46-48] Similar to several literatures, Cu^{2+} ions can enter into B-site of Nb^{5+}/Sb^{5+}, forming $Cu_{Nb/Sb}'''$ defects.[19, 47, 49] According to the characteristics of spectra[50, 51], all KNNSC-*x* ceramics possess two Cu-hyperfine coupling centers of the dimeric $(Cu_{Nb/Sb}''' - V_O^{\bullet\bullet})'$ (DC1) and trimeric $(V_O^{\bullet\bullet} - Cu_{Nb/Sb}''' - V_O^{\bullet\bullet})^{\bullet}$ (DC2) defect combinations. The generation mechanism of the two types of defect combinations can be expressed as **Equation 1**:

$$3CuO \xrightarrow{K_{0.5}Na_{0.5}Nb_{1-x}Sb_xbO_3} (Cu_{Nb/Sb}''' - V_O^{\bullet\bullet})' + (V_O^{\bullet\bullet} - Cu_{Nb/Sb}''' - V_O^{\bullet\bullet})^{\bullet} + Cu_{Na}^{\times} + 3O_O^{\times} \quad (1)$$

In the expression above, $Cu_{Nb/Sb}'''$ and $V_O^{\bullet\bullet}$ severally give three negative charges

and two positive charges, while $Cu_{Na}^{\times}$ and $O_{O}^{\times}$ are in charge neutrality. $Cu_{Na}^{\times}$ is generated by the substitution of Cu^{+} ions in Na^{2+} ions of A-site. As depicted in **Figure 4**f, DC1 consists of one $Cu_{Nb/Sb}^{'''}$ center and one $V_{O}^{\bullet\bullet}$, forming an electric dipole; and DC2 is constituted by one $Cu_{Nb/Sb}^{'''}$ center and two $V_{O}^{\bullet\bullet}$, giving a symmetrical structure without an electric dipole. Furthermore, the charge equilibrium mechanism of KNNSC-*x* ceramics can be described as **Equation 2**:

$$\left[(Cu_{Nb/Sb}^{'''} - V_{O}^{\bullet\bullet})'\right] \approx \left[\left(V_{O}^{\bullet\bullet} - Cu_{Nb/Sb}^{'''} - V_{O}^{\bullet\bullet}\right)^{\bullet}\right] \quad (2)$$

To further obtain the spin-Hamiltonian parameters of two Cu-hyperfine coupling paramagnetic centers and analyze the content evolution of the two sorts of defect combinations with the level of Sb increasing, the EPR spectra (*x* = 0, 0.04 and 0.16) have been simulated, as displayed in **Figure 4**b-d. Consistently with previous reports[19, 46], the obtained spin-Hamiltonian parameters are $g_{zz}^{1} = 2.159$, $A_{zz}^{1} = 294$ MHz for DC1 and $g_{zz}^{2} = 2.199$, $A_{zz}^{2} = 511$ MHz for DC2. With the increasing of Sb content, the resonance peaks of both DC1 and DC2 are weakened, which reflects the significant decrease trend of the content of these two defect combinations. In particular, at *x* = 0.16, the resonance peaks are quite flat, indicating the existence of small quantity of defect combinations in this component. In addition, the spins contents of DC1 and DC2 which represent the concentration of defect combinations have been obtained from the simulation results, as shown in **Figure 4**e. For each component, the concentration of DC2 exceeds that of DC1 because the formation energy of DC2 is less than that of DC1. The DC1 and DC2 give the maximum concentrations of ~5.36×10^{18} spin g^{-1} and ~6.36×10^{18} spin g^{-1} in KNNSC-0

ceramics and their concentrations decrease slightly when the doping amount of Sb increases to 0.04. Furthermore, the concentrations of DC1 and DC2 sharply decrease to the minimum values of ~3.67×10^{18} spin g^{-1} and ~3.96×10^{18} spin g^{-1} when the doping amount of Sb increases to 0.16.

To further investigate the reasons for the reduction of defect combinations, XPS spectra of KNNSC-*x* ceramics are fitted by Lorentzian-Gaussian functions to analyze the content of $V_o^{\bullet\bullet}$ and the valence state of Cu ions. As shown in **Figure 4**g, the O 1*s* spectra are divided into two peaks. The towering peak at ~529.5 eV represents the lattice oxygen, while low and flat one at ~530.9 eV ascribes to the adsorption oxygen that represents the existence of $V_o^{\bullet\bullet}$.[4, 52] Based on the area ratio of the two peaks, the $V_o^{\bullet\bullet}$ content of KNNSC-*x* ceramics can be estimated. It can be seen that the $V_o^{\bullet\bullet}$ content decreases from 16.4% at x = 0 to 14.5% at x = 0.16. For acceptor-doped KNN-based piezoceramics, in addition to the $V_o^{\bullet\bullet}$ induced by the volatilization of K/Na ions, the replacement of acceptor ions for B-site ions can lead to the generation of additional $V_o^{\bullet\bullet}$. Therefore, the reduction of $V_o^{\bullet\bullet}$ should be ascribed to the decline of acceptor ions. As displayed in **Figure 4**h, two species of Cu ions (i.e., Cu^{+} at ~932 eV and Cu^{2+} at ~933 eV) can be detected in KNNSC-*x* ceramics with x = 0 and 0.04.[15, 53] However, only Cu^{+} peak is still observed at x = 0.16, suggesting that Cu^{+} (0.96 Å) ions mainly replace Na^{+} (0.97 Å) ions of A-site so that Cu^{2+} ions are not enough to be detected by XPS in KNNSC-0.16 ceramics.[54] That is, almost all Cu^{2+} ions have been converted to Cu^{+} ions after the addition of high levels of Sb. Macroscopically, the color of KNNSC-*x* ceramics varies from pitch-black to reddish

while *x* rises from 0 to 0.16. By the square, the replacement of Nb^{5+}/Sb^{5+} ions by every two Cu^{2+} ions can induce three $V_O^{\bullet\bullet}$. In other words, the ratio of $Cu_{Nb/Sb}'''$ to $V_O^{\bullet\bullet}$ follows the **Equation 3**:

$$[Cu_{Nb/Sb}'''] : [V_O^{\bullet\bullet}] \approx 1: 1.5 \quad (3)$$

Exactly, the $V_O^{\bullet\bullet}$ content is reduced by ~2% (Figure 4g), while the reduction of Cu^{2+} ions is ~1% (**Figure 4**h), which is very close to ratio of $Cu_{Nb/Sb}'''$ to $V_O^{\bullet\bullet}$. Therefore, the decline of $V_O^{\bullet\bullet}$ content should be ascribed to the reduced substitution of Cu^{2+} for Nb^{5+}/Sb^{5+} in B-site. As a result, the absence of $Cu_{Nb/Sb}'''$ and $V_O^{\bullet\bullet}$ makes it difficult to form enough defect combinations.

3.3 "hard-soft" transformation of ferroelectricity and piezoelectricity

The *I-E* and *P-E* loops of KNNSC-*x* ceramics are depicted in **Figure 5**a-f. Similar to previous reports[55, 56], the CuO-doped KNN ceramic, i.e., *x* = 0, exhibits an almost completely constricted double ferroelectric hysteresis loop with a saturation polarization (P_s) of ~19.8 μC cm^{-2} and a remnant polarization (P_r) of ~0 μC cm^{-2}, while its *I-E* loop displays four leakage current peaks, indicating the strongly hardening characteristic.[57] The double ferroelectric hysteresis loop in CuO-doped KNN is resulted from the restoring force provided by defect dipoles. In the loading process of electric field, it is difficult for the defect dipoles to follow the reversal of electric field. Accordingly, the ferroelectric domain returns to the initial position under the restoring force provided by the defect dipole when the electric field is removed.[58] It has been proved that the content of defect combinations, especially DC1, is considered as a key factor to affect the contraction degree of *P-E* loops. The

double ferroelectric hysteresis loop is gradually opened with increasing *x*, indicating that the softening characteristic is increasingly prominent. Moreover, KNNSC-0.04 ceramics present a transition state with a slight contraction of ferroelectric hysteresis loop (**Figure 5**d) because of the existence of a small amount of defect combinations, manifesting that KNNSC-0.04 ceramics may exhibit "semihard" properties (**Figure S2**). While *x* further increases (**Figure 5**d-f), typical saturated single ferroelectric hysteresis loops are observed and the *I-E* curves present only two flat current peaks, indicating the conventional switching of ferroelectric domains due to the decrease in the concentration of DC1 and DC2. The well-saturated and square-like single ferroelectric hysteresis loops (x = 0.08 and 0.16) are similar to pure KNN ceramics. For KNNSC-0.16 ceramics, the ferroelectricity is weaker than that of KNNSC-0.08 ceramics due to the existence of the impurity phase (**Figure 1**). However, its E_c is smaller than that of KNNSC-0.08 ceramics, which illustrates that it is easier for the domains to flip with electric fields. In a word, for KNNSC-*x* ceramics, after adding Sb, the defect content reduces, leading to the gradual opening of the double hysteresis loop which indicates the "hard to soft" transformation of ferroelectric behaviors in the ceramics.

For acceptor-doped KNN-based ceramics, ferroelectric domains of poled ceramics can't be reversed completely in variational AC electric field directions due to the existence of defect dipole and thus the ceramics give an offset ferroelectric loops with unequal coercive field $|E_c^+|$ and $|E_c^-|$.[15] The E_c and the internal bias field E_i are severally calculated by **Equation 4** and **5**:

$$E_c = \frac{E_c^+ - E_c^-}{2} \quad (4)$$

$$E_i = \frac{E_c^+ + E_c^-}{2} \quad (5)$$

As presented in **Figure 5**g and h, poled KNNSC-0 ceramic exhibits an almost completely off-center hysteresis loop, presenting the fairly large E_c of ~9.7 kV cm^{-1} and E_i of ~8.21 kV cm^{-1}. However, the observed E_c and E_i significantly decrease with the intake of Sb. At x = 0.16, the observed E_c and E_i are very low (E_c: ~4.86 kV cm^{-1}, E_i: ~1.63 kV cm^{-1}), revealing that the ceramics with x = 0.16 are obviously softened.

As shown in **Figure 6**a, the planar electromechanical coupling factor k_p firstly increases from 35.3% to 45.4% as x increases from 0 to 0.04 and then remains above 40% with further increasing x. It is well known that the d_{33} is closely related to $\varepsilon_r P_r$ (P_r here represents the remnant polarization of the poled ceramic). Obviously, the d_{33} and $\varepsilon_r P_r$ show a highly consistent trend, that is, both the d_{33} and $\varepsilon_r P_r$ increase with x increasing (**Figure 6**a). In detail, the d_{33} increases from 85 pC N^{-1} at x = 0 to 218 pC N^{-1} at x = 0.16. In addition to the R-O phase boundary at room temperature, the gradual decrease of defect dipoles is responsible for the enhancement of d_{33}. As displayed in **Figure 6**b, KNNSC-x ceramics with x < 0.08 possess a relatively low *tan*δ (< 0.5%). With x further increasing, the *tan*δ increases beyond 1%. However, the Q_m and θ show the opposite trend to *tan*δ. At x = 0, the ceramic exhibited an ultrahigh Q_m (~2426). However, the Q_m greatly decreases while x increases from 0 to 0.16, giving a very low Q_m (~142) at x = 0.16. Obviously, the introduction of Sb greatly softens Cu-doped KNN-based ceramics. This softening effect has been reported in CuO-doped KNN-based modified with Sb-containing compositions such as

$Li(Nb_{0.5}Sb_{0.5})O_3$ and $LiSbO_3$ (**Table 1**). It can be seen that compared to the CuO-modified KNN ceramic without Sb doping, the ceramic with x = 0.16 exhibit significant softened piezoelectricity (d_{33}~218 pC N^{-1} and Q_m~142), which is similar to the ceramic of $0.95(K_{0.5}Na_{0.5}NbO_3)$-$0.05Li(Nb_{0.5}Sb_{0.5})O_3$ + 0.8 mol% CuO (d_{33}~207 pC N^{-1} and Q_m~320). The θ value also continues to decrease from 88.8° to 80.3° as x increases from 0 to 0.16. Declined Q_m and increased d_{33} indicate that the ceramics have been significantly softened after the addition of Sb. As shown in **Figure 2** and **Figure 4**, the R-O phase transition temperature gradually get closer to room temperature and defect combinations continues to decrease with x increasing, resulting in enhanced d_{33} and reduced Q_m.

4. Conclusion

Sb-modified KNN ceramics with CuO doping were prepared by a traditional ceramic technique, and the crystal structure, microscopic morphology, defect structure and electric properties of KNNSC-x ceramics have been systematically studied. The ferroelectric and piezoelectric properties of KNNSC-x ceramics exhibit a hardening-softening transformation after adding Sb. The KNNSC-0 ceramics (i.e., without Sb doping) exhibit extremely hardening characteristics, i.e., pinched ferroelectric loops with P_r of ~0 μC cm^{-2}, ultrahigh Q_m of ~2426, and low $tan\delta$ of 0.32%, etc. However, with the introduction of Sb, KNNSC-x ceramics are gradually softened, giving fairly softening characteristics, such as saturated single P-E hysteresis loop with a large P_r and excellent piezoelectric property (d_{33} > 210 pC N^{-1}).

Our results reveal that the decrease of defect dipoles in the ceramics reduces the restoring force on ferroelectric domains and thus results in the decrease of Q_m. In summary, the content of defect combinations can directly and significantly influence the evolution of ferroelectric and piezoelectric properties in KNNSC-*x* ceramics.

Acknowledgments

Authors gratefully acknowledge the supports from the projects of National Natural Science Foundation of China (Grant Number 51572178), Sichuan Science and Technology Program (2016JY0225). Y. Liao and D. Wang appreciate the support of National Undergraduate Innovation and Entrepreneurship Training Program (201810636045, Sichuan Normal University).

References

[1] H.L. Tuller, S.R. Bishop, Point Defects in Oxides: Tailoring Materials Through Defect Engineering, Annu. Rev. Mater. Res., 41 (2011) 369-398.

[2] B. Jaffe, W.R. Cook, H.L. Jaffe, Piezoelectric Ceramic, Academic Press, London and New York, 1971.

[3] P.K. Panda, B. Sahoo, PZT to Lead Free Piezo Ceramics: A Review, Ferroelectrics, 474 (2015) 128-143.

[4] Y. Guo, P. Xiao, R. Wen, Y. Wan, Q. Zheng, D. Shi, K.H. Lam, M. Liu, D. Lin, Critical roles of Mn-ions in enhancing the insulation, piezoelectricity and multiferroicity of $BiFeO_3$-based lead-free high temperature ceramics, J. Mater. Chem. C, 3 (2015) 5811-5824.

[5] S.Y. Chu, T.Y. Chen, I.T. Tsai, W. Water, Doping effects of Nb additives on the piezoelectric and dielectric properties of PZT ceramics and its application on SAW device, Sens. Actuators, A, 113 (2003) 198-203.

[6] A. Garg, D.C. Agrawal, Effect of rare earth (Er, Gd, Eu, Nd and La) and bismuth additives on the mechanical and piezoelectric properties of lead zirconate titanate ceramics, Mater. Sci. Eng., B, 86 (2001) 134-143.

[7] B.H. Chen, C.L. Huang, L. Wu, Promotion of piezoelectric properties of lead zirconate titanate ceramics with (Zr,Ti) partially replaced by Nb_2O_5, Solid-State Electron., 48 (2004) 2293-2297.

[8] A. Tawfik, Elastic Properties and Sound Wave Velocity of PZT Transducers Doped with Ta and La, J. Am. Ceram. Soc., 68 (2010) C-317-C-319.

[9] Y.A. Genenko, J. Glaum, M.J. Hoffmann, K. Albe, Mechanisms of aging and fatigue in ferroelectrics, Mater. Sci. Eng., B, 192 (2015) 52-82.

[10] S. Takahashi, Effects of impurity doping in lead zirconate-titanate ceramics, Ferroelectrics, 41 (1982) 143-156.

[11] S.-M. Lee, S.-H. Lee, C.-B. Yoon, H.-E. Kim, K.-W. Lee, Low-temperature sintering of MnO_2-doped PZT-PZN Piezoelectric ceramics, J. Electroceram., 18 (2007) 311-315.

[12] X. Chao, D. Ma, R. Gu, Z. Yang, Effects of CuO addition on the electrical responses of the low-temperature sintered $Pb(Zr_{0.52}Ti_{0.48})O_3$-$Pb(Mg_{1/3}Nb_{2/3})O_3$-$Pb(Zn_{1/3}Nb_{2/3})O_3$ ceramics, J. Alloys Compd., 491 (2010) 698-702.

[13] C. Eric, Materials science: Lead-free at last, Nature, 432 (2004) 24.

[14] M.-H. Zhang, K. Wang, J.-S. Zhou, J.-J. Zhou, X. Chu, X. Lv, J. Wu, J.-F. Li, Thermally stable piezoelectric properties of (K, Na)NbO_3-based leadfree perovskite with rhombohedral-tetragonal coexisting phase, Acta Mater., 122 (2017) 344-351.

[15] T. Wang, D. Wang, Y. Liao, Q. Zheng, H. Sun, K.W. Kwok, N. Jiang, W. Jie, C. Xu, D. Lin, Defect structure, ferroelectricity and piezoelectricity in Fe/Mn/Cu-doped $K_{0.5}Na_{0.5}NbO_3$ lead-free piezoelectric ceramics, J. Eur. Ceram. Soc., 38 (2018) 4915-4921.

[16] S. Zhang, R. Xia, L. Lebrun, D. Anderson, T.R. Shrout, Piezoelectric materials for high power, high temperature applications, Mater. Lett., 59 (2005) 3471-3475.

[17] T. Wang, L. He, Y. Deng, Q. Zheng, F. Xie, C. Xu, D. Lin, Defect-driven evolution of piezoelectric and ferroelectric properties in $CuSb_2O_6$-doped $K_{0.5}Na_{0.5}NbO_3$ lead-free ceramics, J. Am. Ceram. Soc., 100 (2017) 5610-5619.

[18] T. Wang, L. He, Y. Deng, Q. Zheng, Q. Li, N. Jiang, C. Xu, X. Cao, D. Lin, Origin of superior hardening properties in $KCuTa_3O_9$-doped $K_{0.5}Na_{0.5}NbO_3$ lead-free piezoelectric ceramics, Ceram. Int., 43 (2017) 15666-15677.

[19] T. Wang, Y. Liao, D. Wang, Q. Zheng, J. Liao, F. Xie, W. Jie, D. Lin, Cycling- and heating-induced evolution of piezoelectric and ferroelectric properties of CuO-doped $K_{0.5}Na_{0.5}NbO_3$ ceramic, J. Am. Ceram. Soc., 102 (2019) 351-361.

[20] C. Liu, D.Q. Xiao, J.G. Wu, Z. Wang, F.X. Li, T. Huang, J.G. Zhu, Electrical Properties of CuO-doped $(K_{0.5}Na_{0.5})(Nb_{0.92}Sb_{0.03}Ta_{0.05})O_3$ Piezoelectric Ceramics with High Q_m, Ferroelectrics, 458 (2014) 31-36.

[21] Z.-Y. Shen, Y. Xu, J.-F. Li, Enhancement of Q_m in CuO-doped compositionally optimized Li/Ta-modified (Na,K)NbO_3 lead-free piezoceramics, Ceram. Int., 38 (2012) S331-S334.

[22] Y. Zhao, Y. Zhao, R. Huang, R. Liu, H. Zhou, Effect of Sintering Temperature on Microstructure and Electric Properties of $0.95(K_{0.5}Na_{0.5})NbO_3$–$0.05Li(Nb_{0.5}Sb_{0.5})O_3$ with Copper Oxide Sintering Aid, J. Am. Ceram. Soc., 94 (2011) 656-659.

[23] Q. Hu, H. Du, W. Feng, C. Chen, Y. Huang, Studying the roles of Cu and Sb in $K_{0.48}Na_{0.52}NbO_3$ lead-free piezoelectric ceramics, J. Alloy. Compd., 640 (2015) 327-334.

[24] R.X. Huang, Y.Z. Zhao, X.W. Zhang, Y.J. Zhao, R.Z. Liu, H.P. Zhou, Low-Temperature Sintering of CuO-Doped $0.94(K_{0.48}Na_{0.535})$ NbO_3–$0.06LiNbO_3$ Lead-Free Piezoelectric Ceramics, J. Am. Ceram. Soc., 93 (2010) 4018-4021.

[25] R. Zuo, J. Fu, D. Lv, Y. Liu, Antimony Tuned Rhombohedral-Orthorhombic Phase Transition and Enhanced Piezoelectric Properties in Sodium Potassium Niobate, J. Am. Ceram. Soc., 93 (2010) 2783-2787.

[26] W. Hua, Z. Xia, J. Xu, C. Yuan, C. Zhou, Effects of CuO doping on the structure and properties lead-free KNN-LS piezoelectric ceramics, J. Mater. Sci. - Mater. Electron., 24 (2013) 2469-2472.

[27] L.B. Mccusker, R.B. Von Dreele, D.E. Cox, D. Louër, P. Scardi, Rietveld refinement guidelines, J. Appl. Crystallogr., 32 (1999) 36-50.

[28] B.H. Toby, EXPGUI, a graphical user interface for GSAS, J. Appl. Crystallogr., 34 (2001) 210-213.

[29] Y. Liao, D. Wang, H. Wang, T. Wang, X. Wei, D. Lin, Defect-induced transformation between hardening and softening behaviors in CuF_2-doped $K_{0.5}Na_{0.5}NbO_3$ piezoceramics, Ceram. Int., 45 (2019) 2644-2652.

[30] J.L.S. Emeterio, Determination of electromechanical coupling factors of low Q piezoelectric resonators operating in stiffened modes, IEEE Trans. Ultrason. Ferroelectr. Freq. Control, 44 (1997) 108.

[31] H.-Y. Park, I.-T. Seo, M.-K. Choi, S. Nahm, H.-G. Lee, H.-W. Kang, B.-H. Choi, Microstructure and piezoelectric properties of the CuO-added $(Na_{0.5}K_{0.5})(Nb_{0.97}Sb_{0.03})O_3$ lead-free piezoelectric ceramics, J. Appl. Phys., 104 (2008) 034103.

[32] J. Wu, H. Tao, Y. Yuan, X. Lv, X. Wang, X. Lou, Role of antimony in the phase structure and electrical properties of potassium–sodium niobate lead-free ceramics, RSC Adv., 5 (2015) 14575-14583.

[33] D. Lin, K.W. Kwok, H.L.W. Chan, Phase transition and electrical properties of $(K_{0.5}Na_{0.5})(Nb_{1-x}Ta_x)O_3$ lead-free piezoelectric ceramics, Appl. Phys. A, 91 (2008) 167-171.

[34] I.-H. Chan, C.-T. Sun, M.-P. Houng, S.-Y. Chu, Sb doping effects on the piezoelectric and ferroelectric characteristics of lead-free $Na_{0.5}K_{0.5}Nb_{1-x}$ Sb_xO_3 piezoelectric ceramics, Ceram. Int., 37 (2011) 2061-2068.

[35] B. Orayech, A. Faik, G.A. López, O. Fabelo, J.M. Igartua, Mode-crystallography analysis of the crystal structures and the low- and high-temperature phase transitions in $Na_{0.5}K_{0.5}NbO_3$, J. Appl. Crystallogr., 48 (2015) 318-333.

[36] A.W. Hewat, Cubic-tetragonal-orthorhombic-rhombohedral ferroelectric transitions in perovskite potassium niobate: neutron powder profile refinement of the structures, J. Phys. C: Solid State Phys., 6 (2001) 2559-2572.

[37] H. Watelet, J.P. Picard, G. Baud, J.P. Besse, R. Chevalier, Classement des porteurs de charge et conductivite du compose $K_8Na_4Sb_{12}O_{36}$ de structure $KSbO_3$ cubique, Mater. Res. Bull., 16 (1981) 877-882.

[38] L. Jiang, Y. Li, X. Jie, J. Wu, C. Qiang, L. Hong, D. Xiao, J. Zhu, Phase structure and enhanced piezoelectric properties in $(1-x)(K_{0.48}Na_{0.52})(Nb_{0.95}Sb_{0.05})O_3$-$x(Bi_{0.5}Na_{0.42}Li_{0.08})_{0.9}Sr_{0.1}ZrO_3$ lead-free piezoelectric ceramics, Ceram. Int., 43 (2016).

[39] R.D. Shannon, Revised effective ionic radii and systematic studies of interatomic distances in halides and chalcogenides, Acta Crystallogr., Sect. A: Found. Crystallogr., 32 (1976) 751-767.

[40] D. Wang, Y. Liao, Z. Peng, Q. Zheng, X. Wei, T. Wang, D. Lin, Defect-relevant piezoelectric and ferroelectric properties in $LiCuTa_3O_9$-doped $K_{0.5}Na_{0.5}NbO_3$ lead-free piezoceramics, J. Mater. Sci. - Mater. Electron., 30 (2019) 2563–2571.

[41] H. Li, W.Y. Shih, W.-H. Shih, Effect of Antimony Concentration on the Crystalline Structure, Dielectric, and Piezoelectric Properties of $(Na_{0.5}K_{0.5})_{0.945}Li_{0.055}Nb_{1-x}Sb_xO_3$ Solid Solutions, J. Am. Ceram. Soc., 90 (2007) 3070-3072.

[42] B. Zhang, J. Wu, X. Cheng, X. Wang, D. Xiao, J. Zhu, X. Wang, X. Lou, Lead-free piezoelectrics based on potassium-sodium niobate with giant d_{33}, ACS Appl.

Mater. Inter., 5 (2013) 7718-7725.

[43] R.-A. Eichel, Characterization of Defect Structure in Acceptor-Modified Piezoelectric Ceramics by Multifrequency and Multipulse Electron Paramagnetic Resonance Spectroscopy, J. Am. Ceram. Soc., 91 (2008) 691-701.

[44] R.-A. Eichel, M.D. Drahus, P. Jakes, E. Erünal, E. Erdem, S.K.S. Parashar, H. Kungl, M.J. Hoffmann, Defect structure and formation of defect complexes in Cu^{2+}-modified metal oxides derived from a spin-Hamiltonian parameter analysis, Mol. Phys., 107 (2009) 1981-1986.

[45] Y. Yan, K.H. Cho, S. Priya, Identification and Effect of Secondary Phase in MnO_2-Doped $0.8Pb(Zr_{0.52}Ti_{0.48})O_3–0.2Pb(Zn_{1/3}Nb_{2/3})O_3$ Piezoelectric Ceramics, J. Am. Ceram. Soc., 94 (2011) 3953-3959.

[46] R.-A. Eichel, E. Erünal, P. Jakes, S. Körbel, C. Elsässer, H. Kungl, J. Acker, M.J. Hoffmann, Interactions of defect complexes and domain walls in CuO-doped ferroelectric $(K,Na)NbO_3$, Appl. Phys. Lett., 102 (2013) 242908.

[47] R.A. Eichel, E. Erunal, M.D. Drahus, D.M. Smyth, J. van Tol, J. Acker, H. Kungl, M.J. Hoffmann, Local variations in defect polarization and covalent bonding in ferroelectric Cu^{2+}-doped PZT and KNN functional ceramics at the morphotropic phase boundary, Phys. Chem. Chem. Phys., 11 (2009) 8698-8705.

[48] E. Erünal, Structural characterization of CuO-doped alkali niobate piezoelectric ceramics by electron paramagnetic resonance spectroscopy, Universität Freiburg, Universität Freiburg, 2011.

[49] R.A. Eichel, Structural and dynamic properties of oxygen vacancies in perovskite

oxides-analysis of defect chemistry by modern multi-frequency and pulsed EPR techniques, Phys. Chem. Chem. Phys., 13 (2011) 368-384.

[50] E. Erünal, R.A. Eichel, J. Acker, H. Kungl, M.J. Hoffmann, Structural Characterization of Cu2+ Functional Centers In 'Lead-Free' KNN Piezoelectrics, Mrs Proceedings, 1199 (2009).

[51] S.M. Ke, H.T. Huang, H.Q. Fan, H.K. Lee, L.M. Zhou, Y.W. Mai, Antiferroelectric-like properties and enhanced polarization of Cu-doped $K_{0.5}Na_{0.5}NbO_3$ piezoelectric ceramics, Appl. Phys. Lett., 101 (2012) 024102.

[52] Z.-T. Li, H. Liu, H.-C. Thong, Z. Xu, M.-H. Zhang, J. Yin, J.-F. Li, K. Wang, J. Chen, Enhanced Temperature Stability and Defect Mechanism of BNT-Based Lead-Free Piezoceramics Investigated by a Quenching Process, Adv. Electron. Mater., 5 (2019) 1800756.

[53] M.C. Biesinger, L.W.M. Lau, A.R. Gerson, R.S.C. Smart, Resolving surface chemical states in XPS analysis of first row transition metals, oxides and hydroxides: Sc, Ti, V, Cu and Zn, Appl. Surf. Sci., 257 (2010) 887-898.

[54] H.-Q. Wang, Y.-J. Dai, X.-W. Zhang, D. Damjanovic, Microstructure and Hardening Mechanism of $K_{0.5}Na_{0.5}NbO_3$ Lead-Free Ceramics with CuO Doping Sintered in Different Atmospheres, J. Am. Ceram. Soc., 95 (2012) 1182-1184.

[55] D. Lin, K.W. Kwok, H.L.W. Chan, Double hysteresis loop in Cu-doped $K_{0.5}Na_{0.5}NbO_3$ lead-free piezoelectric ceramics, Appl. Phys. Lett., 90 (2007) 232903.

[56] X. Tan, H. Fan, S. Ke, L. Zhou, Y.-W. Mai, H. Huang, Structural dependence of piezoelectric, dielectric and ferroelectric properties of $K_{0.5}Na_{0.5}(Nb_{1-2x/5}Cu_x)O_3$

lead-free ceramics with high Q_m, Mater. Res. Bull., 47 (2012) 4472-4477.

[57] W. Pan, Q. Zhang, A. Bhalla, L.E. Cross, Field-Forced Antiferroelectric-to-Ferroelectric Switching in Modified Lead Zirconate Titanate Stannate Ceramics, J. Am. Ceram. Soc., 72 (1989) 571-578.

[58] X. Ren, Large electric-field-induced strain in ferroelectric crystals by point-defect-mediated reversible domain switching, Nat. Mater., 3 (2004) 91-94.

Figures:

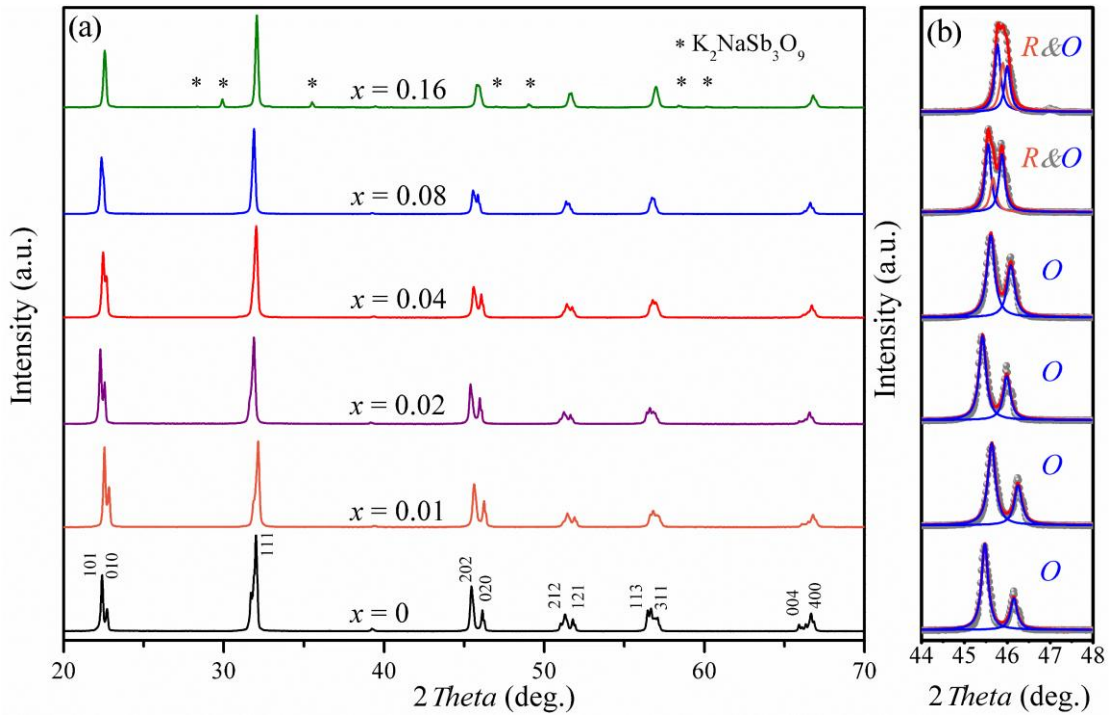

Figure 1. (a) XRD patterns of KNNSC-*x* ceramics, (b) enlarged and simulated XRD patterns in the range of 2θ from 44^{o} to 48^{o}.

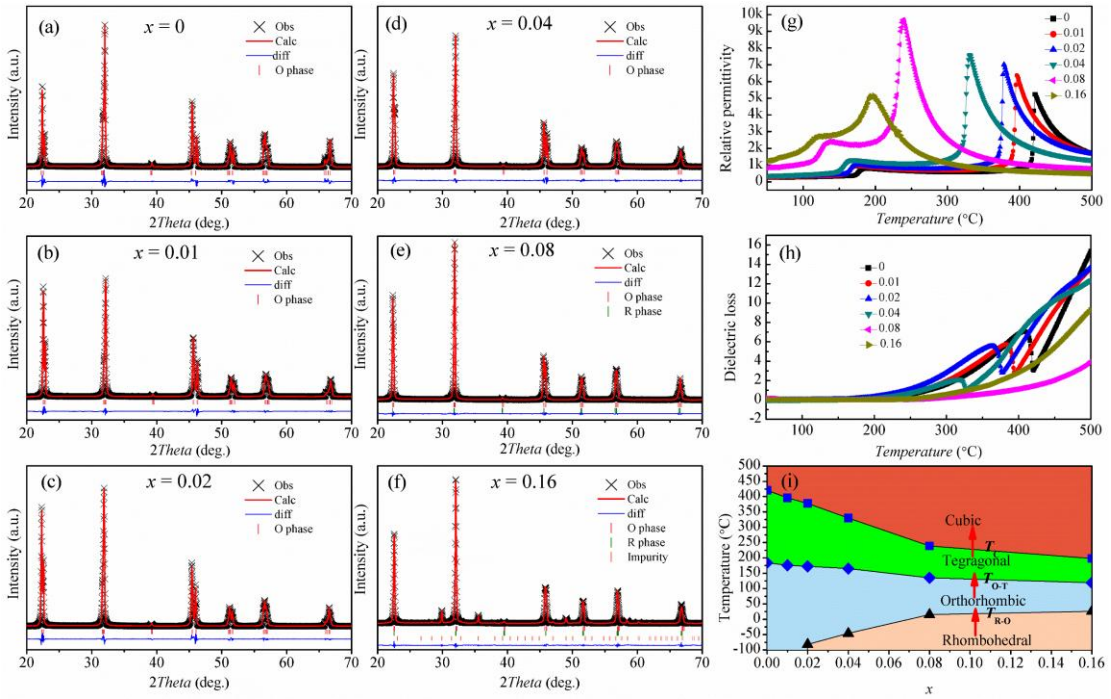

Figure 2. (a-f) XRD refinements of XRD patterns of KNNSC-*x* ceramics, temperature dependences of (g) ε_r and (h) *tan*δ at the temperature range of 50-500 ^{o}C, (i) the phase diagram of KNNSC-*x* ceramics.

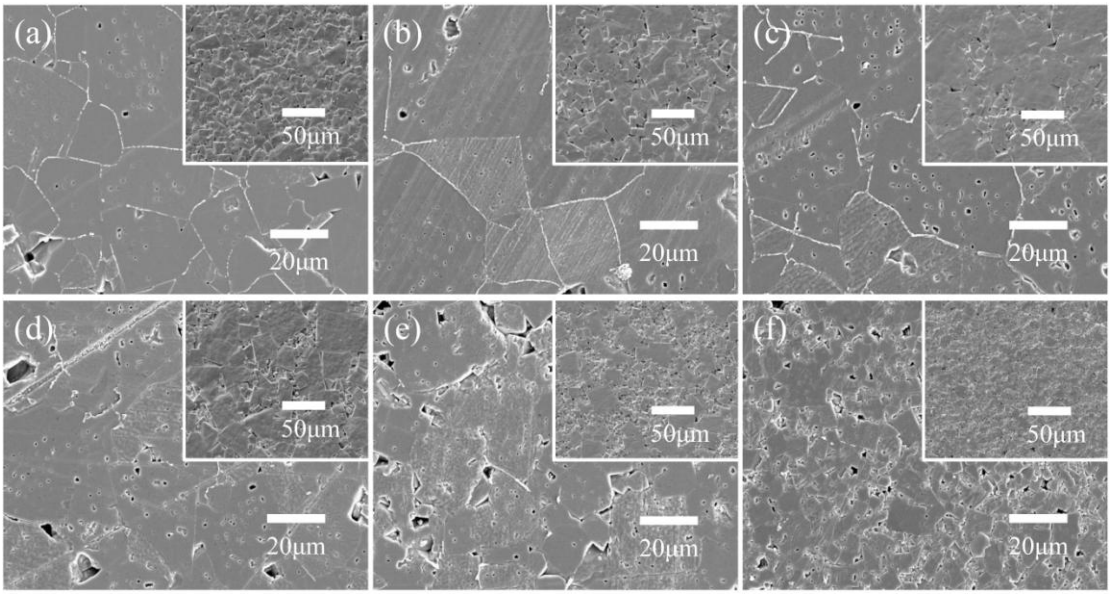

Figure 3. SEM images of thermally etched fracture section after polishing and the surface (inserts) of KNNSC-*x* ceramics with (a) *x* = 0, (b) *x* = 0.01, (c) *x* = 0.02, (d) *x* = 0.04, (e) *x* = 0.08, and (f) *x* = 0.16.

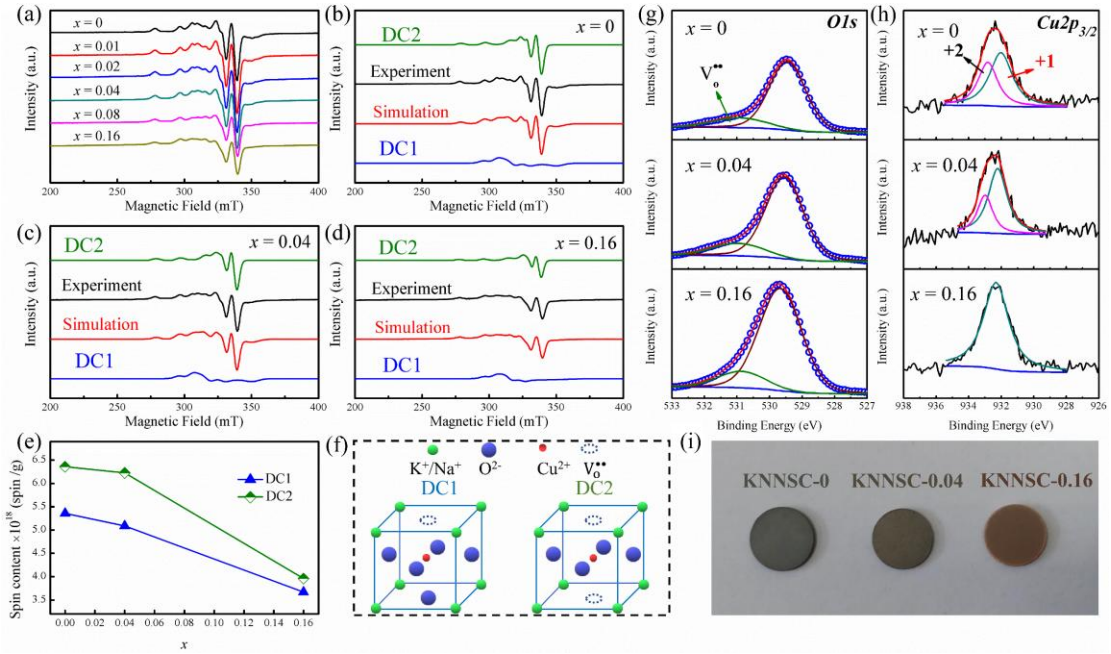

Figure 4. (a) X-band EPR spectra of KNNSC-*x* ceramics; (b-d) simulated EPR spectra; (e) variations of spins concentration of DC1 and DC2 with *x*; (f) schematic views of DC1 and DC2; XPS spectra for (g) O 1*s* and (h) Cu $2p_{3/2}$ of KNNSC-*x* ceramics (*x* = 0, 0.04, and 0.16); (i) real shot diagrams of KNNSC-*x* ceramics (*x* = 0, 0.04, and 0.16).

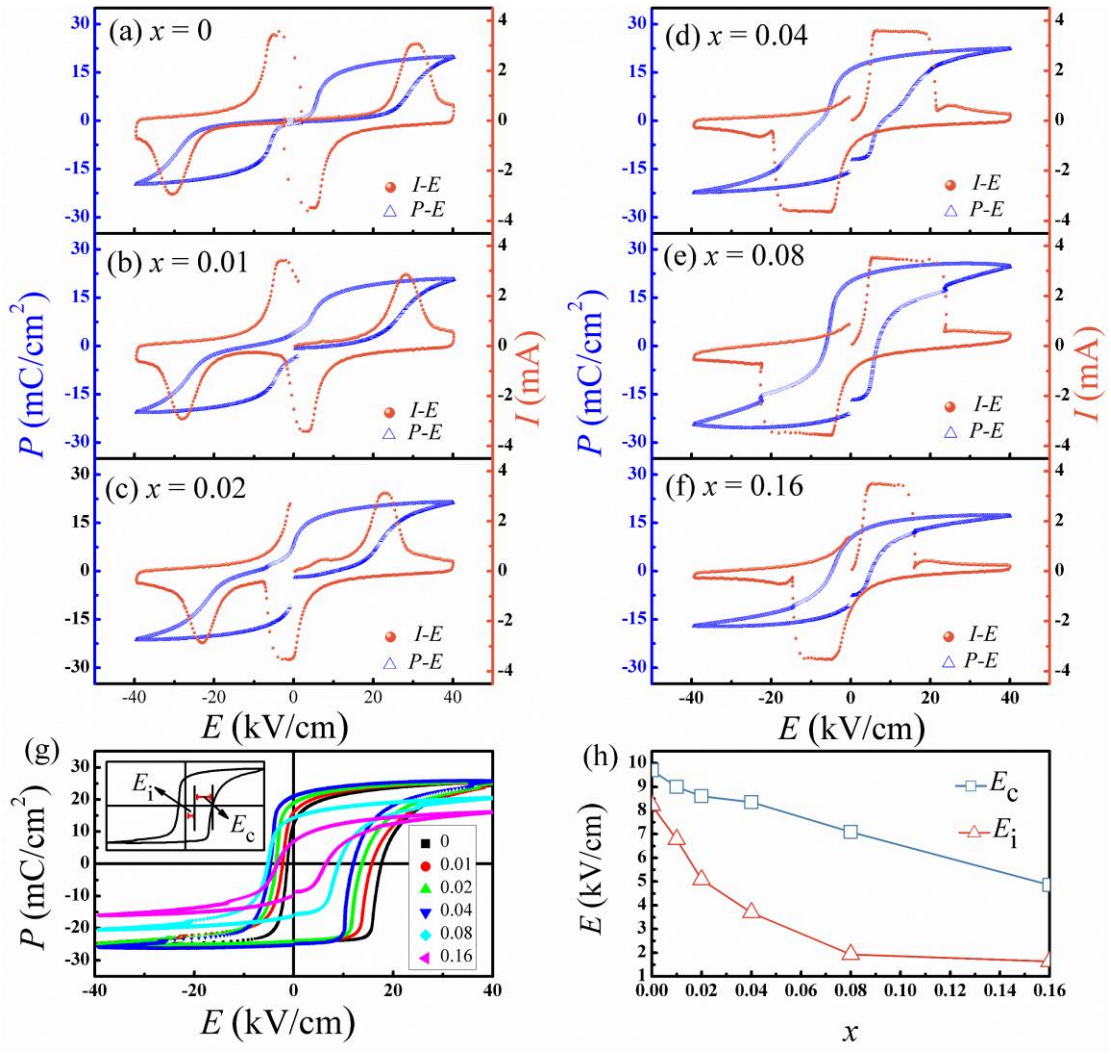

Figure 5. (a-f) *I-E* and *P-E* loops of KNNSC-*x* ceramics (@10 Hz); (g) *P-E* loops of poled KNNSC-*x* ceramics (@10 Hz); (h) variations of E_c and E_i with *x*.

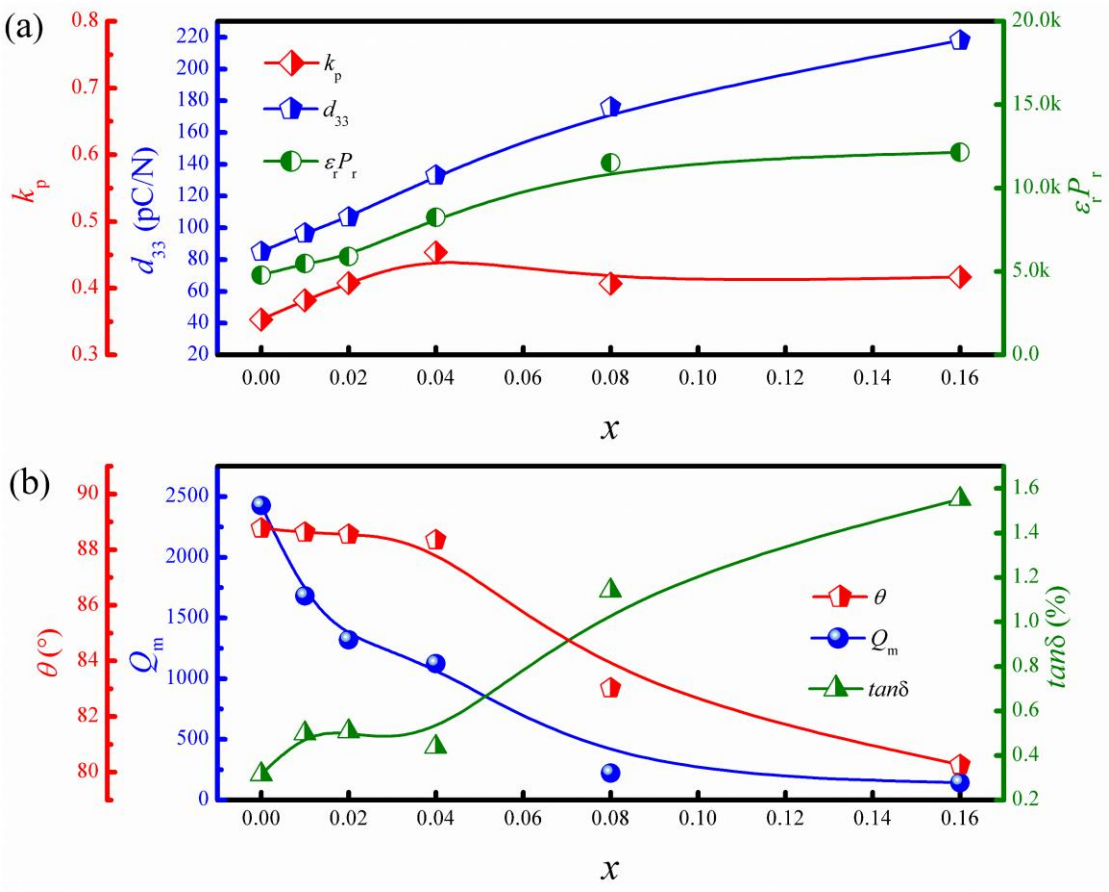

Figure 6. (a) Variations of k_p, d_{33}, and $\varepsilon_r P_r$ with x for the poled KNNSC-x ceramics and (b) variations of θ, Q_m, and $tan\delta$ with x for the poled KNNSC-x ceramics.

Supplemental iInformation

Click here to download e-component: Supplemental Information-R1.docx